Bull. Mater. Sci., Vol. 38, No. 5, September 2015, pp. 1333–1338. © Indian Academy of Sciences.

Transformation from amorphous to nano-crystalline SiC thin films prepared by HWCVD technique without hydrogen dilution

F SHARIATMADAR TEHRANI

Department of Physics, Semnan University, 35195-363 Semnan, Iran

MS received 26 January 2015; accepted 20 April 2015

Abstract. **Silicon carbide (SiC) thin films were deposited on Si(111) by the hot wire chemical vapour deposition (HWCVD) technique using silane (SiH_4) and methane (CH_4) gases without hydrogen dilution. The effects of SiH_4 to CH_4 gas flow ratio (R) on the structural properties, chemical composition and photoluminescence (PL) properties of the films deposited at the different gas flow ratios were investigated and compared. X-ray diffraction (XRD) and Fourier transform infrared (FTIR) spectra revealed a structural transition from amorphous SiC to cubic nano-crystalline SiC films with the increase in the gas flow ratio. Raman scattering confirmed the multi-phased nature of the films. Auger electron spectroscopy showed that the carbon incorporation in the film structure was strongly dependent on the gas flow ratio. A similar broad visible room-temperature PL with two peaks was observed for all SiC films. The main PL emission was correlated to the band to band transition in uniform a-SiC phase and the other lower energy emission was related to the confined a-Si : H clusters in a-SiC matrix. SiC nano-crystallites exhibit no significant contribution to the radiative recombination.**

Keywords. **Nano-crystalline cubic SiC; hot wire CVD; structural properties; photoluminescence.**

1. Introduction

The interest in crystalline silicon carbide (SiC) stems from its potential in various electronic and optoelectronic devices, including solar cells, thin film transistors, blue light-emitting diodes (LEDs), high-power and high-temperature electronic devices.[1] This is due to its unique properties such as wide tunable energy gap, high electron mobility, high thermal conductivity and high break-down field.[2] For application of SiC thin films in the field of Si-based thin film solar cells and thin film transistors with hetero-junction structure low-temperature deposition is desirable. This is necessary to avoid the formation of high density of defects at the SiC/Si interface due to difference in thermal expansion coefficient (8%) and lattice mismatch (20%) between the SiC film and Si substrate.[3] Low-temperature deposition is also advantageous for fabrication of thin film solar cells on substrates with low melting point such as glass, flexible substrates, etc.[3–5]

Crystalline SiC thin films have been produced at low substrate temperature by researchers using various techniques such as plasma-enhanced chemical vapour deposition (PECVD),[6] pulsed laser ablation[7] and reactive magnetron sputtering[5] and hot wire chemical vapour deposition (HWCVD).[4] HWCVD became popular technique due to the simplicity and low operational cost. It also allows deposition of SiC films at low substrate temperatures and high deposition rates.[8,9] HWCVD has the capability of producing high-density radicals from the decomposition of gases by heated filament, resulting in enhancement in the quality of the deposited film. The absence of ion bombardment on the film surface is another added advantage as it reduces defects in the film structure.[10] Generally, in order to deposit SiC films by this technique, different gas sources are employed such as monomethylsilane (MMS)/H_2,[11–15] $SiH_4/CH_4/H_2$,[16–18] $SiH_4/C_2H_2/H_2$[9] and $SiH_4/C_2H_6/H_2$.[19] Amorphous SiC films are usually reported to be formed when C_2H_2 or C_2H_6 is used as the carbon sources,[19,20] while formation of crystalline SiC thin films has been reported mostly from the use of CH_4 and SiH_4 gas mixture[21] or MMS gas sources with high dilution in hydrogen.[12] However, from the viewpoint of cost reduction and practical application, employing SiH_4/CH_4 gas mixture without H_2 could be advantageous because hydrogen dilution tends to reduce the deposition rate of the films.[22–24] To date, there are no reported works on the deposition of nanocrystalline-3C-SiC (nc-3C-SiC) film by the HWCVD technique using only SiH_4 and CH_4. This motivates us to investigate the growth of nano-crystalline SiC at low temperature by HWCVD technique from SiH_4/CH_4 gas mixture without hydrogen dilution. By excluding hydrogen gas in the deposition process, the deposition cost will be reduced due to the remarkable increase in the deposition rate. Also, eliminating this

(shariatmadartehrani@yahoo.com)

highly explosive gas will be resulting in easier handling of the deposition system.

SiH_4 molecules are preferentially decomposed by the heated filament, while the decomposition of CH_4 molecules occurs mainly through secondary gas phase reactions.[16] The gas flow rate into the reaction chamber is an important parameter that controls the composition and structure of the resulting SiC films, as it influences the density of radicals generated and the probability of gas phase reactions. In this paper, the influence of SiH_4 to CH_4 flow rate ratio, R, on the structural, composition and optical properties of SiC films was reported. It was found that the structural transition from amorphous to nanocrystalline occurs with the increase in R above 0.05. It is also shown that all the films exhibit visible photoluminescence (PL) emission at room temperature. The structural change and PL mechanism are discussed.

2. Experimental

The SiC thin films were grown by a home-built HWCVD system on silicon wafers using SiH_4 and CH_4 gas sources. A tungsten wire of 0.5 mm in diameter was coiled into a 20 mm length helix and placed 26 mm above the substrates. The filament was pre-heated up to 2000°C under constant flow rate of H_2 (40 sccm) for 10 min to remove the possible existing oxides prior to deposition. The substrates were placed into the deposition chamber immediately after standard cleaning process. Afterwards, the chamber was pumped down to a base pressure of about 2×10^{-3} Pa. The deposition duration was set for 30 min. During deposition process, the substrate temperature, filament temperature and pressure were kept at 300°C, 1900°C and 80 Pa, respectively, while varying SiH_4 to CH_4 flow rate ratio, defined as $R = [SiH_4]/[CH_4]$, from 0.01 to 0.1. To obtain these ratios, the SiH_4 flow rate was fixed at 1 sccm and the CH_4 flow rates were varied from 10 to 100 sccm.

The X-ray diffraction (XRD) measurement was carried out using SIEMENS D5000 X-ray diffractometer, with CuKα ($\lambda = 1.5418$ Å) to study the crystallinity of the samples. Fourier transform infrared (FTIR) spectroscopy was employed to analyse the chemical bonding properties. FTIR spectra were obtained in the transmission mode within the scanning range from 400 to 4000 cm^{-1} using a Perkin-Elmer System 2000 FTIR spectrometer. The absorption spectra were normalized to the film thickness after subtracting the baseline. The deconvolution of the spectra into the individual peaks was carried out using Origin 8.0 software. Film thickness was measured using a KLA-TENCOR mechanical profilometer and was in the range of about 600–1100 nm. Film composition was acquired from the Auger electron spectroscopy (AES) data, using a Jeol JAMP-9500F field emission Auger microprobe system. Silicon and carbon atomic percentage was determined as the average of the depth profile with Ar^+ ions (5 kV accelerating voltage) sputtering at an etching rate of 14.8 nm min^{-1}. The film structure was further investigated using a Renishaw via Raman Microscope with a 514 nm Ar^+ laser excitation source and the laser power of 10 mW. PL measurement was performed at room temperature using a 325 nm He–Cd laser.

3. Results and discussion

3.1 *XRD*

Figure 1 shows the XRD patterns of the SiC films deposited at various gas flow ratio, R. All films revealed an XRD peak at 2θ of 56.7° corresponding to the crystalline Si (311) orientation plane produced by the Si-substrate. This was confirmed by XRD pattern of bare Si substrate. Three XRD peaks were observed at 2θ of 35.7°, 60.0° and 71.8° corresponding to the (111), (220) and (311) reflection planes of 3C-SiC,[23] respectively. This was found for the films deposited at $R \geq 0.05$, which shows the formation of SiC crystallites in these films. The 3C-SiC crystallite size of these films, estimated using Scherrer's formula,[25] was in the range of 2–6 nm. The samples prepared at R below 0.05 were amorphous.

3.2 *FTIR*

Figure 2 shows the FTIR absorption spectra of the SiC thin films prepared at different R values. The main feature of these spectra was a sharp absorption band in the range of 600–1100 cm^{-1}. This band is contributed by the

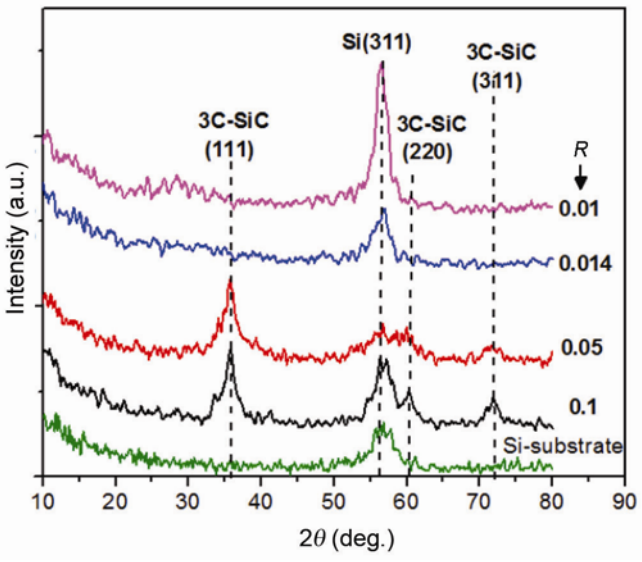

Figure 1. XRD pattern of the films deposited at various R values. Reflection peaks corresponding to Si and 3C-SiC are shown.

superposition of absorption peaks located at about 650, 800 and 980 cm^{-1} corresponding to the Si–H wagging (w), Si–C stretching (str) and C–H wagging (w) vibration modes, respectively.[26] Additionally, a weak absorption band in the range of 1900–2200 cm^{-1} was detected (data not shown), which is attributed to Si–H (str) vibration modes.[27] C–H_n stretching vibration at the range of 2800–3000 cm^{-1},[28] usually observed in hydrogenated a-SiC films, was absent in our spectra. It was observed that the former absorption band increased in intensity and was blue-shifted with the increase in *R*, while the Si–H (str) band follows the opposite trend. The decrease in the Si–H (str) indicates a decrease in the hydrogen concentration in the films prepared at higher *R*. Moreover, the evolution in the shape and width of the Si–C (str) band suggested a phase transformation from amorphous to crystalline[3,5] with the increase in *R*. In order to verify this transformation, standard deconvolutions of this absorption band was carried out. Taking films deposited at lowest and highest *R* as examples are shown in figure 3a and b, respectively. The Si–C (str) band was fitted to both Gaussian and Lorentzian distribution curves to determine the amorphous and crystalline components of the SiC phase in the film structure, respectively. This technique has been adopted widely by many researchers working on SiC films.[3,14,29]. The Lorentzian component of Si–C (str) mode was dominant in the films deposited at higher *R* with insignificant presence of Si–H (w) and C–H (w) modes. The presence of Gaussian Si–C (str), Si–H (w) and C–H (w) modes became more significant compared to the Lorentzian Si–C (str) mode at lower *R*. The SiC crystalline volume fraction of the films prepared at different *R* was estimated following the formula $A_L/(A_G + A_L)$ where A_L and A_G are the areas under Si–C Lorentzian and Gaussian components, respectively. The SiC crystalline volume fraction of the films prepared at *R* of 0.01 and 0.014 is about 4 and 13%, respectively, which are almost amorphous. For the films prepared at highest *R* (0.1) this value considerably increased to about 55% which was consistent with the XRD results.

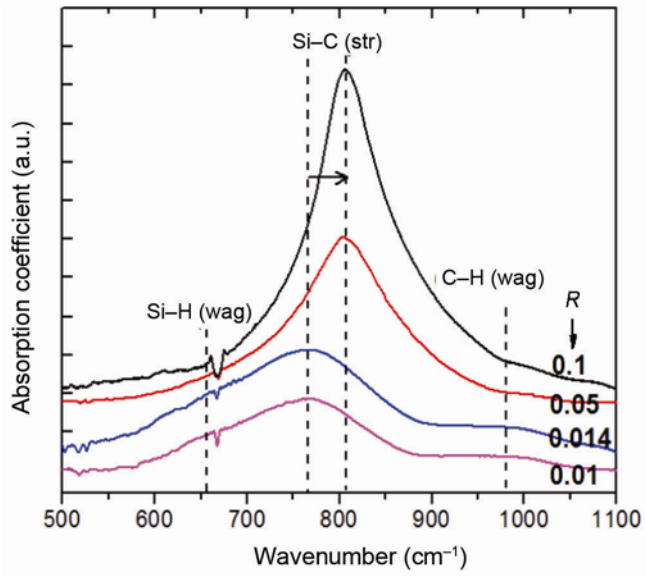

Figure 2. FTIR absorption spectra of SiC films prepared at various gas flow ratios, *R*.

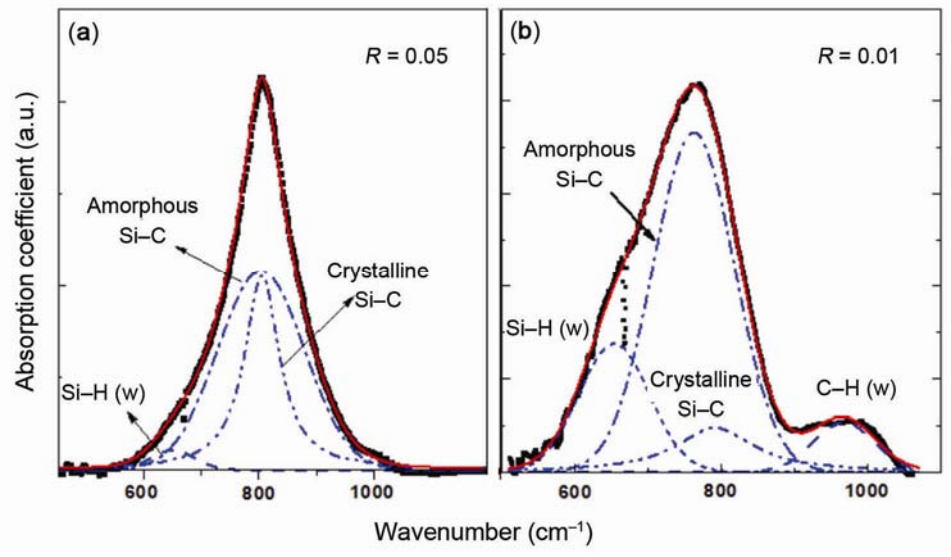

Figure 3. Typical deconvolution of the absorption band centred at ~ 800 cm^{-1} into Si–H (w), Si–C (str) and C–H (w) components for film with (**a**) dominant crystalline and (**b**) amorphous SiC phases. The Gaussian and Lorentzian lines of Si–C peak are representative of amorphous and crystalline phases, respectively.

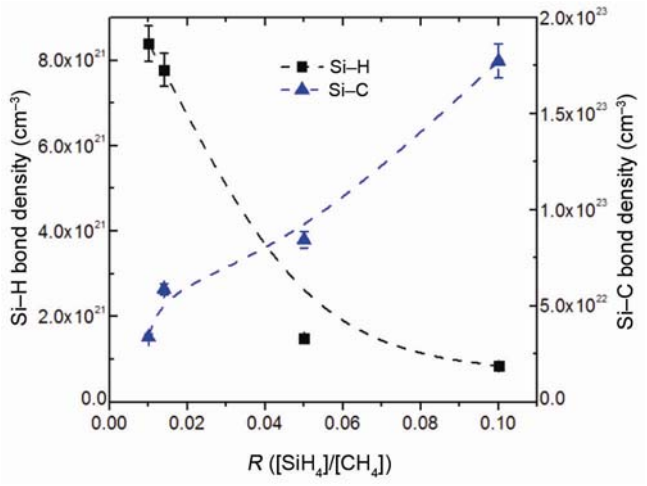

Figure 4. Variation of Si–C and Si–H bond densities with *R* calculated from FTIR spectra.

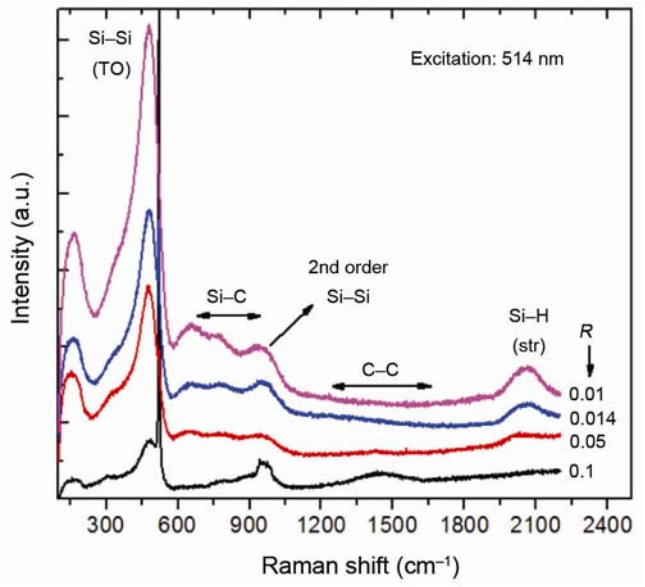

Figure 5. Visible Raman scattering spectra of SiC films prepared at indicated *R*.

The bond density (*N*) of Si–C and Si–H were calculated by using the following formula

$$N = \frac{A}{\nu_0}\int \alpha(\nu)\mathrm{d}\nu,$$

where A, ν_0 and $\alpha(\nu)$ are the reverse cross-section, position of the absorption peak and absorption coefficient, respectively. The standard values of A for Si–C and Si–H stretching vibration modes adopted from literature are 2.13×10^{19} and 1.40×10^{20} cm^{-2}, respectively.[30] Figure 4 shows a decrease in bond density of Si–H and increase in Si–C bond with the increase in *R*. The absence of C–H (str) indicates that there were no a-C : H clusters in the films, while the presence of C–H (wag) vibration mode was associated with the C–H bonds attached to Si atom (Si–C–H).[31] It can be concluded that the films deposited at low *R* are generally amorphous with a mixture of a-Si : H phase embedded within a more dominant a-SiC : H phase, while the films deposited at higher *R* showed lower hydrogen concentration with more ordered Si–C matrix.

3.3 *Raman spectroscopy*

While the Si–C bonds are strongly infrared active, the Si–Si and C–C bonds are silent in the IR spectra. Raman spectroscopy is a powerful tool to identify these symmetric bonds via inelastic Raman scattering due to their high polarizability. Figure 5 shows the visible Raman scattering spectra of the SiC films deposited at different *R*. A sharp peak at 521 cm^{-1} and a broad band near 970 cm^{-1} corresponding to first- and second-order scattering of crystalline Si substrate were seen in the spectra. This is due to the penetration depth of the excitation wavelength which exceeds the films thickness. The broad bands centred at about 170, 350 and 480 cm^{-1} were attributed to TA, LO and TO modes, respectively, of Si–Si in the a-Si phase.[32] The position and the width of these bands did not significantly change with the increase in *R*. It is well known that the width of the Si–Si (TO) mode is directly related to the bond angle deviation and the short range order in the a-Si phase.[33,34] This indicates that the structure of amorphous Si phase in the films is not affected by the *R* variations. The band located in the region between 700 and 1000 cm^{-1}, usually associated with Si–C bonds was weak due to the low Raman efficiency of SiC.[9,35] For the film prepared at highest *R*, a broad band entered at ~1500 cm^{-1} associated with the C–C sp^2 bonds was observed. This band was red-shifted from the position of the G bands of a-C : H films at 1590 cm^{-1},[36,37] due to the addition of Si to the carbon matrix.[38] However, this band was not observed in the other films. Therefore, the corporation of carbon atoms in these films was small and occurred mainly in the forms of Si–C and/or C–H bonds. The formation of multi-phased films consisting of a-SiC, 3C-SiC, a-Si : H and a-C : H and SiC phases was strongly supported by Raman, FTIR and XRD results.

3.4 *AES*

The relative atomic concentrations of silicon, Si, and carbon, C, in the films were obtained from the Auger electron spectroscopy. Figure 6 shows the variation of C content defined as $[100 \times C/(C + Si)]$ with *R*. The C content was less than 50% in all films, indicating that the relative concentration of Si was higher than that of C in all of the SiC thin films studied in this work. The increase in *R* up to 0.1 increased the C content in the films. These results showed that C incorporation into the film structure

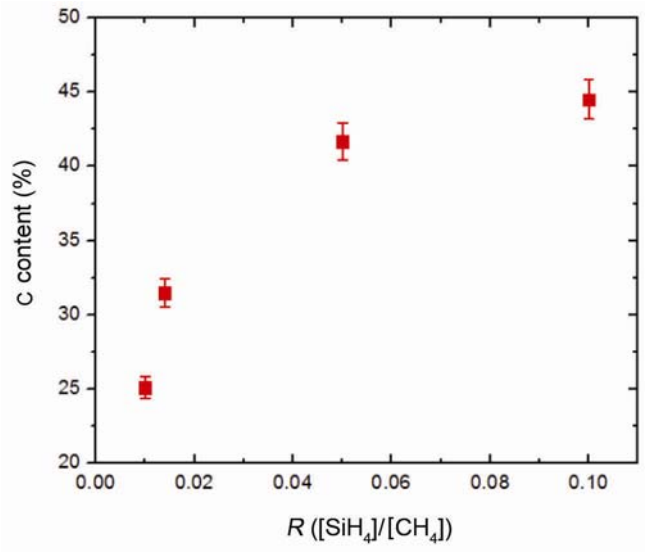

Figure 6. Dependence of carbon content of the films defined as C/(C + Si) on *R*.

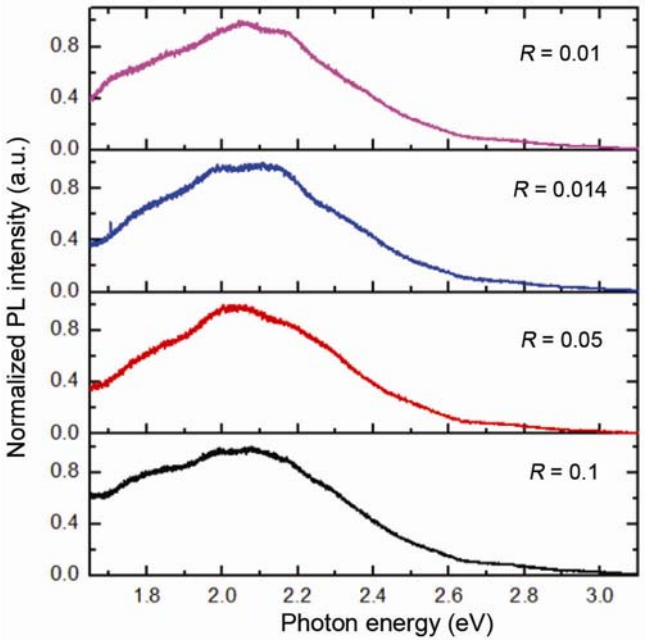

Figure 7. Normalized room-temperature PL spectra for films deposited under different *R*, excited using 325 nm laser.

was strongly influenced by the partial pressure of CH_4 with respect to the SiH_4 gas. High density of H radicals generated from decomposition of SiH_4 gas by the heated W-filament go through secondary gas-phase reactions with the CH_4 molecules and enhances the density of C-related radicals reaching the growth sites. The increase in *R* decreased the partial pressure of SiH_4 gas and consequently limited the number of Si and H radicals generated during SiH_4 decomposition by the hot filament and thus reduced the density of C-related radicals reaching the growth sites.

The films deposited at the higher *R* showed the nearest stoichiometric composition. However, the latter films were inhomogeneous and consisted of a-Si : H, a-C : H and a-SiC : H phases as confirmed by Raman and FTIR results. These results differ from those reported by Hoshide *et al*[24] in their work on HWCVD SiC films. They showed that decreasing *R* from 1 to 0.5 resulted in an amorphous film structure. However, the configuration of our deposition system and the different parameters such as pressure and filament temperature used in this work enabled nc-SiC film structure to be grown at much lower *R*.

3.5 *PL spectroscopy*

Figure 7 shows the room-temperature PL spectrum of the SiC films deposited at various *R*. Broad PL bands were observed for all films in the visible range centred at about 2.07 eV with a broad shoulder at about 1.75 eV.

The presence of amorphous and nc-SiC as well as a-Si : H and rarely a-C : H phases was observed in our films, in which a transition from amorphous to nc-SiC was evident with the increase in *R*. However, no significant shift or broadening can be seen in the PL spectra with increase in *R*. This suggested that the mechanism of the PL emission was similar for all the films and nc-SiC does not contribute to radiative recombination. As both a-SiC and a-Si : H were dominant phases in our films, the PL spectra could be attributed to them. It has been reported that amorphous SiC films exhibit PL emission and the peak position and FWHM were shown to be strongly dependent on the carbon incorporation where increase in C content produced a blue shift and broadening of the PL peak.[9] We correlated the main PL peak (~ 2.07 eV) to the band to band transition of electrons in the a-SiC phase. This PL energy is consistent with the reported bandgap of a-SiC films with relatively low C content (about 30%).[39] The constant position and width of the PL peak implied that the C content in the a-SiC phase was similar in all films, despite the higher C incorporation at higher *R*. This is because C atoms were spread into both amorphous and crystalline phases and their content may not be changed in the amorphous SiC phase.

On the other hand, it is commonly accepted that photoluminescent emission from a-Si : H films is absent at room temperature because of thermal quenching effect as a result of high-density paramagnetic defects (dangling bonds), which act as nonradiative recombination centres.[40] However, theoretical calculations have shown that decrease in the size of a-Si : H clusters resulted in a blue-shift in PL peak position and increase in intensity due to the improvement of PL efficiency of confined a-Si : H.[41] By considering the presence of a-Si : H with similar structural ordering among all these films seen from Raman results,

one can associate the lower energy PL emission (1.75 eV) to the spatial confinement of this phase within the dominant a-SiC matrix. As the energy gap of the a-Si : H was much lower than that of a-SiC, confinement of electrons within a quantum well may contribute to the direct transition and radiative recombination in the a-Si : H clusters.

4. Conclusion

SiC thin films were prepared using the HWCVD technique from a mixture of SiH_4 and CH_4 gases without hydrogen dilution. The films containing SiC nano-crystallite and high-density Si–C bonds were formed at $R = ([SiH_4]/[CH_4])$ above 0.05. This was the lower limit of R which allowed the formation of SiC nano-crystallites. We found that the density of H radicals produced from SiH_4 dissociation contributed to the CH_4 decomposition and etching of amorphous phases and consequently, determined the composition and the structure of the deposited SiC films. The production of H radicals reaching the growth sites in HWCVD process could be controlled by the R. Visible room-temperature PL was observed with main peak at 2.07 eV and a broad shoulder at 1.75 eV for all SiC films. The energy and width of the PL peaks did not change significantly with R. The mechanism of PL emissions at high and low energy was correlated to the unaffected a-SiC and confined a-Si : H phases in the films respectively.

References

1. Hamakawa Y, Matsumoto Y, Hirata G and Okamoto H 1989 *MRS Proc.* **164** 291
2. Matsunami H and Kimoto T 1997 *Mater. Sci. Eng.* **R20** 125
3. Rajagopalan T 2003 *J. Appl. Phys.* **94** 5252
4. Komura Y, Tabata A, Narita T, Kondo A and Mizutani T 2006 *J. Non-Cryst. Solids* **352** 1367
5. Kerdiles S 2000 *Appl. Phys. Lett.* **76** 2373
6. Forhan N A E, Fantini M C A and Pereyra I 2004 *J. Non-Cryst. Solids* **338–340** 119
7. Nainaparampil J J and Zabinski S J 1999 *J. Vac. Sci. Technol. A* **17** 909
8. Komura Y, Tabata A, Narita T and Kondo A 2008 *Thin Solid Films* **516** 633
9. Swain B P and Dusane R O 2006 *Mater. Chem. Phys.* **99** 240
10. Gogoi P, Jha H S and Agarwal P 2010 *Thin Solid Films* **518** 6818
11. Kaneko T, Hosokawa Y, Suga T and Miyakawa N 2006 *Microelectron. Eng.* **83** 41
12. Chen T, Köhler F, Heidt A, Huang Y, Finger F and Carius R 2011 *Thin Solid Films* **519** 4511
13. Miyajima S, Irikawa J, Yamada A and Konagai M 2010 *Appl. Phys. Lett.* **97** 023504
14. Finger F, Astakhov O, Bronger T, Carius R, Chen T, Dasgupta A, Gordijn A, Houben L, Huang Y, Klein S, Luysberg M, Wang H and Xiao L 2009 *Thin Solid Films* **517** 3507
15. Klein S, Carius R, Finger F and Houben L 2006 *Thin Solid Films* **501** 169
16. Tabata A and Komura Y 2007 *Surf. Coat. Technol.* **201** 8986
17. Zhao Q, Li J C, Zhou H, Wang H, Wang B and Yan H 2004 *J. Cryst. Growth* **260** 176
18. Mao H-Y, Wuu D-S, Wu B-R, Lo S-Y, Hsieh H-Y and Horng R-H 2012 *Thin Solid Films* **520** 2110
19. Itoh T, Fujiwara T, Katoh Y, Fukunaga K and Nonomura S 2002 *J. Non-Cryst. Solids* **299–302** 880
20. Swain B P and Dusane R O 2006 *Microelectron. Eng.* **83** 55
21. Tabata A, Komura Y, Narita T and Kondo A 2009 *Thin Solid Films* **517** 3516
22. Tabata A and Mori M 2008 *Thin Solid Films* **516** 626
23. Tabata A, Hoshide Y and Kondo A 2010 *Mater. Sci. Eng. B* **175** 201
24. Hoshide Y, Komura Y, Tabata A, Kitagawa A and Kondo A 2009 *Thin Solid Films* **517** 3520
25. Klug H P and Alexander L E 1974 *X-ray diffraction procedures for polycrystalline and amorphous materials* (Wiley: New York)
26. Hartel A M, Künle M, Löper P, Janz S and Bett A W 2010 *Sol. Energy Mater. Sol. Cells* **94** 1942
27. Chew Rusli K, Yoon S F, Ahn J, Ligatchev V, Teo E J, Osipowicz T and Watt F 2002 *J. Appl. Phys.* **92** 2937
28. Ritikos R, Siong C C, Ab Gani S M, Muhamad M R and Rahman S A 2009 *Jpn. J. Appl. Phys.* **48** 101301
29. Yu W, Wang X, Lu W, Wang S, Bian Y and Fu G 2010 *Physica B: Condens. Matter* **405** 1624
30. Kaneko T, Nemoto D, Horiguchi A and Miyakawa N 2005 *J. Cryst. Growth* **275** e1097
31. Vasin A V, Kolesnik S P, Konchits A A, Rusavsky A V, Lysenko V S, Nazarov A N, Ishikawa Y and Koshka Y 2008 *J. Appl. Phys.* **103** 123710
32. Smith Jr J E, Brodsky M H, Crowder B L, Nathan M I and Pinczuk A 1971 *Phys. Rev. Lett.* **26** 642
33. Beeman D, Tsu R and Thorpe M F 1985 *Phys. Rev. B* **32** 874
34. Wang Y, Yue R and Liu L 2002 *Appl. Surf. Sci.* **193** 138
35. Cheng Q *et al* 2008 *J. Phys. D: Appl. Phys.* **41** 055406
36. Ferrari A C and Robertson J 2000 *Phys. Rev. B* **61** 14095
37. Ferrari A C and Robertson J 2004 *Philos. Trans. R. Soc. Lond. A* **362** 2477
38. Guruvenket S, Azzi M, Li D, Szpunar J A, Martinu L and Klemberg-Sapieha J E 2010 *Surf. Coat. Technol.* **204** 3358
39. Rerbal K, Jomard F, Chazalviel J N, Ozanam F and Solomon I 2003 *Appl. Phys. Lett.* **83** 45
40. Dunstan D J and Boulitrop F 1984 *Phys. Rev. B* **30** 5945
41. Estes M J and Moddel G 1996 *Phys. Rev. B* **54** 14633